Front. Earth Sci. 2018, 12(1): 160–169
https://doi.org/10.1007/s11707-017-0626-3

RESEARCH ARTICLE

Live microbial cells adsorb Mg^{2+} more effectively than lifeless organic matter

Xuan QIU[1,2], Yanchen YAO[2], Hongmei WANG (✉)[1,2], Yong DUAN[2]

1 State Key Laboratory of Biogeology and Environmental Geology, China University of Geosciences, Wuhan 430074, China
2 School of Environmental Studies, China University of Geosciences, Wuhan 430074, China

Abstract The Mg^{2+} content is essential in determining different Mg-$CaCO_3$ minerals. It has been demonstrated that both microbes and the organic matter secreted by microbes are capable of allocating Mg^{2+} and Ca^{2+} during the formation of Mg-$CaCO_3$, yet detailed scenarios remain unclear. To investigate the mechanism that microbes and microbial organic matter potentially use to mediate the allocation of Mg^{2+} and Ca^{2+} in inoculating systems, microbial mats and four marine bacterial strains (*Synechococcus elongatus*, *Staphylococcus* sp., *Bacillus* sp., and *Desulfovibrio vulgaris*) were incubated in artificial seawater media with Mg/Ca ratios ranging from 0.5 to 10.0. At the end of the incubation, the morphology of the microbial mats and the elements adsorbed on them were analyzed using scanning electronic microscopy (SEM) and energy diffraction spectra (EDS), respectively. The content of Mg^{2+} and Ca^{2+} adsorbed by the extracellular polysaccharide substances (EPS) and cells of the bacterial strains were analyzed with atomic adsorption spectroscopy (AAS). The functional groups on the surface of the cells and EPS of *S. elongatus* were estimated using automatic potentiometric titration combined with a chemical equilibrium model. The results show that live microbial mats generally adsorb larger amounts of Mg^{2+} than Ca^{2+}, while this rarely is the case for autoclaved microbial mats. A similar phenomenon was also observed for the bacterial strains. The living cells adsorb more Mg^{2+} than Ca^{2+}, yet a reversed trend was observed for EPS. The functional group analysis indicates that the cell surface of *S. elongatus* contains more basic functional groups (87.24%), while the EPS has more acidic and neutral functional groups (83.08%). These features may be responsible for the different adsorption behavior of Mg^{2+} and Ca^{2+} by microbial cells and EPS. Our work confirms the differential Mg^{2+} and Ca^{2+} mediation by microbial cells and EPS, which may provide insight into the processes that microbes use to induce Mg-carbonate formation.

Keywords microbe, adsorption, magnesium, calcium

Received May 22, 2016; accepted October 9, 2016

E-mail: hmwang@cug.edu.cn, wanghmei04@163.com

1 Introduction

Mg-bearing calcium carbonates (Mg-$CaCO_3$) are important minerals on Earth because they constitute a large fraction of the total carbonate reservoir and compose the skeleton of most marine invertebrates (Xu et al., 2013). It is widely accepted that the variation of mineral phases in sedimentary carbonates is highly associated with the fluctuation of oceanic hydrochemical conditions during the Phanerozoic eon (Sandberg, 1983; McKenzie and Vasconcelos, 2009). The Mg/Ca ratio of the ocean (Mg/$Ca_{solution}$) is considered to be the most essential hydrochemical variable (Folk and Land, 1975; Mucci and Morse, 1983; Saunders et al., 2014). Low Mg-calcite ($Mg < 4\%$, hereafter molar percent) is mainly formed in oceans with low Mg/Ca ratios, and high Mg-calcite ($Mg > 4\%$) mainly precipitates in oceans with high Mg/$Ca_{solution}$ (> 2.0). The very high Mg-carbonate, dolomite ($Mg = 50\%$), is also considered to be formed in settings with high Mg/$Ca_{solution}$ (> 5.0; Folk and Land, 1975). Thus, the ratio of Mg/Ca in carbonate minerals was proposed to be indicative of the Mg/Ca ratio in the ocean (Dickson, 2002; Ries et al., 2008).

Nevertheless, the high Mg/$Ca_{solution}$ alone does not guarantee the formation of high Mg-calcite or dolomite. It has been widely accepted that dolomite cannot be precipitated via pure inorganic processes, despite the extremely high Mg/$Ca_{solution}$ (99) and high saturation index respected to dolomite (> 1000) as well as long reaction time (32 years) (Land, 1998). The incorporation of Mg^{2+} into calcite was found to be very difficult because the high binding energy between Mg^{2+} and H_2O impedes the dehydration of the Mg^{2+}–H_2O complex (Chave et al., 1962). In addition, the substitution of Ca^{2+} by Mg^{2+} in calcite would increase the instability of the mineral (Chave et al., 1962) and thus lead to the transformation of high Mg-calcite (Mg > 10%) to other relatively stable solid phases, such as low Mg-calcite or aragonite (Reeder and Sheppard, 1984).

High Mg-$CaCO_3$ has been found in various natural sediments associated with microorganisms, such as organic-rich deposits of the continent margin (50 mol% Mg) (Baker and Burns, 1985), microbialites in the central Pacific Ocean (7–16 mol% Mg) (Camoin et al., 1999), and stromatolite in a Brazil lagoon (40 mol% Mg) (Spadafora et al., 2010). These findings indicated the essential role of microbes and organic matter in the formation of high Mg-$CaCO_3$. Laboratory studies have also demonstrated that both microbes (Krause et al., 2012) and organic matter (Bontognali et al., 2014) are able to induce the formation of high Mg-$CaCO_3$. Microbial mineralization processes are highly associated with their metabolic activities, which lead to an increased saturation index of Mg-$CaCO_3$. For example, cyanobacteria enhance the pH of their surroundings by photosynthesis, while sulfate reducing bacteria (SRB) release Mg^{2+} from the Mg^{2+}–SO_4^{2-} complex by consuming sulfate ions. However, more complex scenarios may exist because the non-metabolizing microbial organism functioned above our expectation in inducing carbonate formation. For example, the amount of carbonate precipitation induced by dead cells of SRB was equal to or even more than that of live cells (Bosak and Newman, 2003). The intact non-metabolizing cells of halophilic archaea or its lysed solution were able to precipitate dolomite, yet metabolizing cells were not capable of doing so (Kenward et al., 2013). These observations suggested something beyond metabolic activities was involved in microbial mineralization that we still did not know.

Both metabolizing microbes and non-metabolizing microbial organisms can adsorb metals in solution via the functional groups with negative charges, such as carboxyl, phosphoryl, and sulfo groups (Braissant et al., 2007). Although the adsorption capacities of functional groups for metals were demonstrated differently by numerous literatures (Wang et al., 2009), it remains unknown whether metabolizing microbes and non-metabolizing microbial organisms behave differently in the adsorption of Mg^{2+} and Ca^{2+}. Since adsorption of Mg^{2+} and Ca^{2+} by microbes or EPS was the first step of biotic formation of high Mg calcite and dolomite, answers to this issue will provide more constraints for both the evaluation of microbial effects in the formation of Mg-contained carbonate and the application of Mg/Ca in microbialites as an indicator for paleoenvironment reconstruction (Ries et al., 2008).

In this study, batch culture experiments were conducted to elucidate the different behaviors of live cells and organic matter of microbial mats and bacterial strains in adsorbing Mg^{2+} and Ca^{2+} in solution with varied Mg/Ca ratios. Our results will offer detailed information about the allocation of Mg^{2+} and Ca^{2+} in a system with microbial cells and microbial organic matter, which is beneficial for understanding of microbially mediated carbonate formation.

2 Materials and methods

2.1 Microbial mat and bacterial strains used

The microbial mat was collected from the Dadeng saltern in Xiamen, China (24°33.832′N, 118°17.646′E). The sampling area was oversaturated with salt, and the water-sediment interface was covered with a green mat. The bacterial community in the mat was analyzed with 16S rRNA clone library construction. In total, four bacterial strains were used in our study. Two aerobic heterotrophic bacteria (*Staphylococcus* sp. and *Bacillus* sp.) were isolated from the microbial mat and subjected to the subsequent experiments. The other two strains used were *Synechococcus elongatus* FACHB-410 (a cyanobacterium), purchased from the Institute of Hydrobiology of the Chinese Academy of Science, and *Desulfovibrio vulgaris* ATCC29579 (a sulfate reducing bacteria), provided by Hailiang Dong from the Miami University.

2.2 Subculture of the microbial mat and bacterial strains

The modified artificial seawater medium (MASW) was used to subculture the microbial mat. The components of 1 L MASW were as follows: NaCl 22.33 g, $MgCl_2$ 5.25 g, $CaCl_2$ 1.18 g, KCl 0.74 g, Na_2CO_3 0.32 g, Na_2SO_4 4.15 g, $NaNO_3$ 1.00 g, KH_2PO_4 39.00 mg, Na_2EDTA 4.50 mg, $FeCl_3$ 0.35 mg, $MnCl_2$ 0.16 mg, $ZnCl_2$ 16.70 μg, $CoCl_2$ 6.50 μg, V_{B1} 0.12 mg, V_{B12} 0.10 mg, and 30 mL of soil extraction. The procedures for preparing the soil extraction are described in Stoupin et al. (2012); V_{B1} and V_{B12} were filtered through a 0.22-μm nitrocellulose membrane before being added to the sterile medium. The ASW, LB, and lactate media were prepared to maintain the cyanobacterium, aerobic heterotrophic bacteria, and SRB, respectively. All media were amended to have a total salinity of 35‰ by altering the dosage of NaCl. The details about the ASW and Lactate media are described in Qiu et al. (2012) and Liu et al. (2012), respectively. Incubation conditions for these cultures are listed in Table 1.

2.3 Microbial mat adsorption experiments

The microbial mat adsorption experiments were conducted in MASW with Mg/Ca ratios of 1.5, 2.5, and 5.2. The various Mg/Ca ratios were achieved by changing the

Table 1 Growth conditions of the microbial mat and bacterial strains in this study

Material	Temperature/°C	Rotation/rpm	Illumination/lux
Microbial mat	25	0	2,000
S. elongatus	25	170	2,000
Staphylococcus sp.	37	170	0
Bacillus sp.	37	170	0
D. vulgaris	37	0	0

dosage of $MgCl_2$ while fixing the amount of $CaCl_2$. The salinities were also fixed to 35‰ by varying the amounts of NaCl. Fresh microbial mats were rived into fragments by sterilized tweezers in an ultraclean benchtop. An aliquot of 2.00 mL of this fragment-containing slurry was inoculated into a beaker with 400 mL of MASW medium. The experiments with dead controls (the microbial mat sterilized at 121°C for 30 mins fully covered the bottom of the beaker) and chemical controls (without microbial mat) were conducted simultaneously. The experiments were terminated when the bottom of the beaker was fully covered with newly growing microbial mats, which took 40 days. The solid phase of each group was collected by centrifugation at 9000 × *g* for 10 min. After discarding the supernatant, centrifugation was conducted again to thoroughly remove the residual solution. The final pellets were subsequently freeze-dried and stored at 4°C for future use. The morphology and the amounts of Mg^{2+} and Ca^{2+} adsorbed by the microbial mat were subsequently analyzed.

2.4 Bacterial strain adsorption experiments

Four bacteria strains were cultured in the media described above with Mg/Ca ratios of 0.5, 1.5, 2.5, 5.2, and 10.0. An aliquot of a 4.0 mL log-phase culture of *S. elongatus*, *Staphylococcus* sp., and *Bacillus* sp. was inoculated into 400 mL fresh medium, and a 15.0 mL culture of *D. vulgaris* was inoculated into 1500 mL medium to obtain sufficient biomass. Duplicates were prepared for each group. The duration from the inoculation to a stable phase was 12 days, 3 days, 3 days, and 30 days for *S. elongatus*, *Staphylococcus* sp., *Bacillus* sp., and *D. vulgaris*, respectively. The native cell (hereafter cell) of the stable phase was collected by centrifugation at 9000 × *g* for 10 min. After discarding the supernatant, centrifugation was conducted again to thoroughly remove the residual solution. The soluble EPS (hereafter EPS) in the supernatant was extracted by adding two volumes of precooled (4°C) ethanol, and the mixture was placed in a refrigerator at 4°C for 12 h. The EPS was collected from the bottom of the beaker using the same processes as for the pellet of the cell. Both cell and EPS were freeze-dried for 20 h and then preserved in a drying vessel at room temperature for further use.

2.5 Analysis methods

2.5.1 Morphology and elemental distribution

The morphology and Mg^{2+} and Ca^{2+} distributions of the microbial mat were analyzed by scanning electronic microscopy (SEM) and energy diffraction spectra (EDS), respectively. The dried microbial mats were rived into small pieces with sharp tweezers. Several pieces of the mats were then adhered onto SEM stubs with double-sided conductive tape. The stubs were coated with Pt for image observation using a FEI Quanta 450 FEG scanning electron microscope (FEI, Hillsboro, America) and SDD Inca X-Max 50 X-ray energy diffraction spectra (OXFORD, London, Britain). The accelerating voltages of the SEM and EDS were 5 kV and 20 kV, respectively.

2.5.2 Cation concentration analysis

To analyze the amount of Mg^{2+} and Ca^{2+} adsorbed on the cell and EPS, 100 mg of the dried cell and EPS of each strain were individually transferred to 5-mL glass vials, and 3.0 mL concentrated HCl (11.9 M) were added. The vials were covered with lids and heated in a water bath at 95°C for 3 h. The acidolyzed product was completely transferred to a volumetric flask and then diluted with double-distilled water (ddH_2O) to 50.00 mL.

The concentrations of Mg^{2+} and Ca^{2+} in the nitrolysis solution were measured with atomic absorption spectroscopy (AAS, Hitachi, 180-70 polarized Zeeman, Japan). The amounts of Mg^{2+} and Ca^{2+} adsorbed by the cell and EPS per one liter of culture were calculated based on Eq. (1).

$$M_{\text{adsorbed by organic matter}} = 2 \times 10^3 \; M_{\text{in nitrolysis solution of organic matter}}, \quad (1)$$

M indicates the concentration of Mg^{2+} or Ca^{2+}, and organic matter is the cell or EPS.

2.5.3 Functional group analysis

To characterize the functional groups on the surface of the cell and EPS, automatic potentiometric titration was conducted on the *S. elongatus* cell and EPS because cyanobacteria were the dominant species in the microbial mat used. Cell and EPS were harvested with the methods mentioned in section 2.4. The pellets of the cell were resuspended in NaCl solution with a final wet cell concentration of 1.645 g/L and a final salinity of 35‰ (NaCl concentration of 0.60 mol/L). The final salinity of the resuspension was equal to that of the medium in which *S. elongatus* were cultured. The pellets of EPS were dissolved in a NaCl-solution with a final wet EPS concentration of 0.724 g/L and a final NaCl concentration of 0.01 mol/L. A volume of 40 mL cell or EPS-suspension was used for the automatic potentiometric titration (Metrohm 902 Titrando, Swiss Land). Hydrochloric acid (HCl) with a concentration of 0.100 mol/L was added into the suspension with an aliquot of 5 μL per step to acidize the solution until a final pH of 2.50 was reached. Then, 0.107 mol/L NaOH solution was added to alkalize the suspension with an aliquot of 5 μL per step until a final pH of 10.50 was reached. The real-time pH of the suspension was recorded during acidification and alkalization. The data obtained from titration were analyzed with Protofit 2.1 under a non-electrostatic adsorption model. The buffer zone and capacity of the material in the solution were automatically estimated with Protofit 2.1 based on the curve between the added volume of acid/base and the change of pH. The buffer zone indicates the possible functional groups and the buffer capacity quantifies the amount of certain functional groups (Turner and Fein, 2006).

3 Results

3.1 Mg^{2+} and Ca^{2+} adsorbed by the microbial mat

3.1.1 Morphology of the cyanobacteria mat

Newly growing microbial mats covered the entire bottom of each beaker after incubation for 40 days. The live microbial mats were characterized by long strips (Fig. 1(a)) with a thick EPS matrix (5–10 μm; Fig. 1(b), black rectangle). These long strips were assemblages of cyanobacterial cells affiliated with *Phormidium*, as indicated by 16S rRNA sequencing (unpublished data). The sterilized microbial mats were partly degraded; few integrated cyanobacteria assemblages were observed (Fig. 1(c)). EPS matrix and single globular cells (Fig. 1(d), white arrow) were observed. Only a small amount of amorphous solid phase was found under chemical control (Figs. 1(e) and 1(f)).

3.1.2 Mg^{2+} and Ca^{2+} adsorbed by the microbial mat

Figure 2 shows the mole percentage of Mg^{2+} and Ca^{2+} on the dried mats and control samples obtained from EDS analysis. The percentages of Mg^{2+} adsorbed by the live mats ($Mg_{\text{live mat}}$) are discrete, varying from 0% to 19.1%. In contrast, the percentages of Mg^{2+} adsorbed by the dead mat ($Mg_{\text{dead mat}}$) or chemical control ($Mg_{\text{chemical control}}$) show a very limited range of $<4\%$. Overall, most of the percentages of $Mg_{\text{live mat}}$ were higher than that of $Mg_{\text{dead mat}}$ and $Mg_{\text{chemical control}}$ (Figs. 2(a), 2(c), and 2(e)). Furthermore, the ratios of Mg/Ca adsorbed by live mats ($Mg/Ca_{\text{live mat}}$) were higher than that of the dead mats ($Mg/Ca_{\text{dead mat}}$) and chemical control ($Mg/Ca_{\text{chemical control}}$; Figs. 2(b), 2(d), and 2(f)). Almost all Mg/Ca ratios over 1.0 appeared in the live mat samples, with only two exceptions observed for the dead mats. It should be noted that higher percentages of $Mg_{\text{live mat}}$ and ratios of $Mg/Ca_{\text{live mat}}$ were observed in samples collected in media with high Mg/Ca ratio (5.2) than in media with low Mg/Ca ratios (2.5 and 1.5). However, this trend was not observed for the dead mats or the chemical controls.

3.2 Mg^{2+} and Ca^{2+} adsorbed by the cell and EPS

The content of Mg^{2+} adsorbed by live cells per unit mass is higher than that of Ca^{2+} in all strains (Figs. 3(a), 3(b), 3(c), and 3(d)), yet the reversed phenomenon was observed for EPS (Figs. 3(e), 3(f), 3(g), and 3(h)). The mole ratios of Mg^{2+} to Ca^{2+} adsorbed on the cell are generally above 1.0 (Figs. 3(j), 3(k), 3(l)) and higher than that of the original medium (values were above the dotted lines), with only one exception (Fig. 3(m)). In contrast, nearly all values of Mg/Ca adsorbed on EPS are below 1.0 (Figs. 3(n), 3(o), 3(p), and 3(q)) and lower than the original Mg/Ca ratio of the medium. The cell of *S. elongatus* shows the highest ability in adsorbing Mg^{2+} (1.55–2.85 mmol/g, Fig. 3(a)). Conversely, the EPS of *S. elongatus* demonstrates the lowest adsorption capacity of Mg^{2+} (<0.20 mmol/g, Fig. 3(e)). The adsorption capacities of Mg^{2+} and Ca^{2+} by the EPS of *Staphylococcus* sp. (Fig. 3(g)) and *Bacillu*s sp. (Fig. 3(h)) are similar to those of the organic matter in the LB medium (Fig. 3(i)).

3.3 Functional groups on the cell surface and EPS of *S. elongatus*

Carboxyl, phosphoryl, and amine groups are estimated to be the major functional groups of EPS and the cell surface of *S. elongatus*. EPS is characterized by acidic (carboxyl) and neutral (phosphoryl) functional groups, with a percentage of 83.08% (Table 2). Conversely, the cell surface is dominated by basic (amine) functional groups, and the total percentage of acidic functional groups (carboxyl and phosphoryl) is estimated to be 12.76% (Table 2).

4 Discussion

4.1 The metabolizing cells adsorb more Mg^{2+} than the non-metabolizing cells

In this study, we found that metabolizing cells adsorbed more Mg^{2+} than Ca^{2+}. Although few publications reported this phenomenon before, clues could still be drawn from related studies. It was observed that the increase of the Mg^{2+} concentration from 0.001 mol/L to 0.1 mol/L causes the much larger decrease of the electrophoretic mobilities

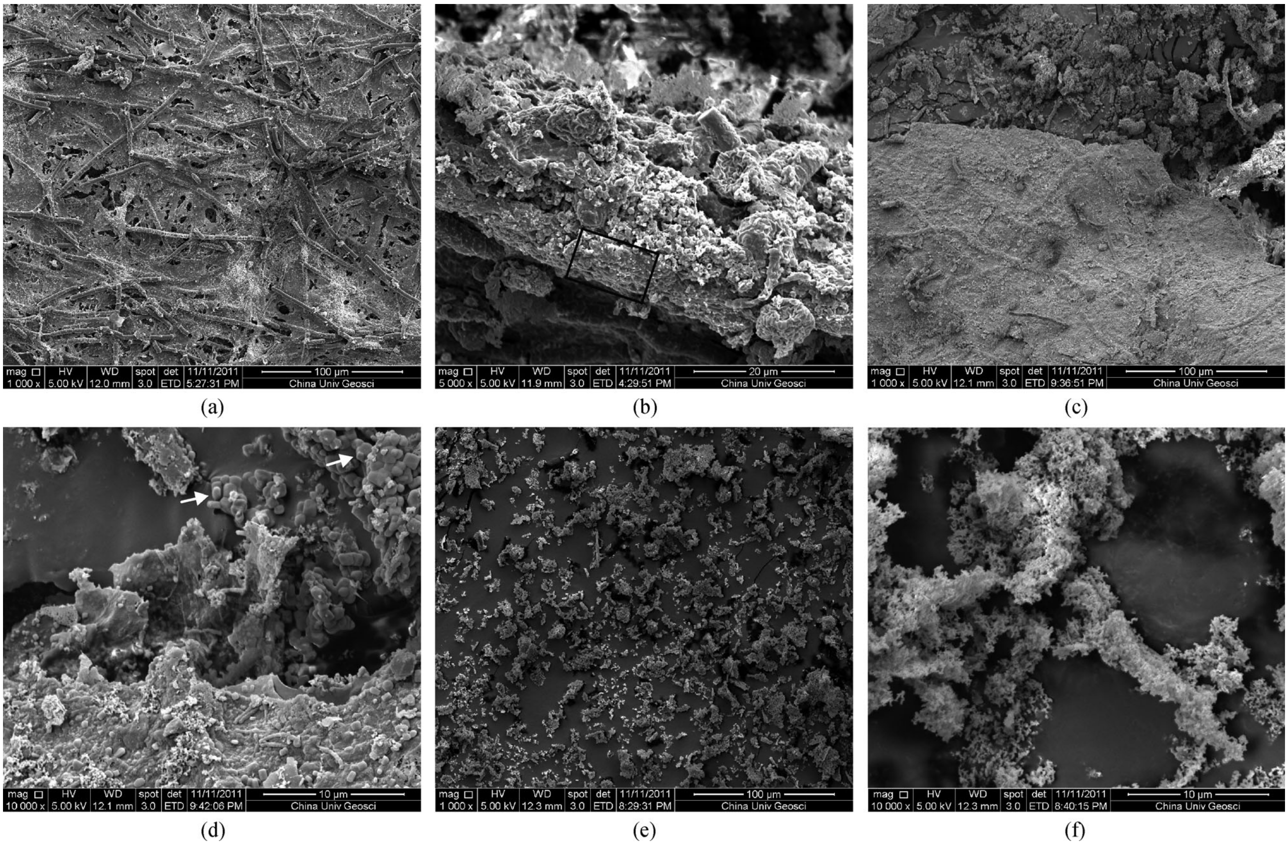

Fig. 1 SEM images of live microbial mats ((a) and (b)), dead microbial mats ((c) and (d)) and the precipitates formed under chemical controls ((e) and (f)). Figs. 1(b), 1(d), and 1(f) are zoomed-in views of Figs. 1(a), 1(c) and, 1(e), respectively.

of the two SRB strains than that from Ca^{2+}, which indicated the higher affinity of the cell surface to Mg^{2+} than to Ca^{2+} (Van Lith et al., 2003). The Mg/Ca ratios on the cell surfaces were always higher than 1.0, and also higher than that in the initial solution after suspending the metabolizing cells of *Methanobacterium formicicum* in the solutions with Mg/Ca ratios varying from 1.0 to 5.2 for 30 min (Kenward et al., 2013). This also suggested that the cell surface of live *M. formicicum* prefers to adsorb Mg^{2+} rather than Ca^{2+}, which coincides with the results in this study conducted on *S. elongatus*, *D. vulgaris*, and *Staphylococcus* sp. (Fig. 3).

In fact, metabolizing cells require more Mg^{2+} than Ca^{2+}. Mg^{2+} is largely and approximately equally required by both the outside wall and inside protoplast (Clapham, 2007) for stabilizing the cell wall, surface layer, cell membrane, ribosomes, and neutralizing nucleic acids as well as assisting enzymatic reactions as a cofactor (Groisman et al., 2013). In contrast, Ca^{2+} was generally extruded outside the cells to maintain a low concentration of approximately 100 nM on the inside, which was 10,000 times lower than that of the outside (Michiels et al., 2002; Clapham, 2007). The need of low Ca^{2+} concentration in the cytoplasm may require a low density of Ca^{2+} on the cell surface. Consequently, the relatively high ratio of Mg/Ca appeared on the cell, which was consistent with the observation from live microbe mats in this study (Fig. 2). The ease of Ca^{2+} precipitation with phosphate also limited the concentration of Ca^{2+} on the cell surface and inside the cell. The precipitation of $Ca_3(PO_4)_2$ may be fatal for the integrity and function of the phospholipid bilayer and nucleic acids (Clapham, 2007). This limitation of Ca^{2+} for live cells no longer exists after the death of the cell, which may facilitate the allocation of Ca^{2+} inside the cell, and subsequently causes the relatively low Mg/Ca ratio of the whole dead cell (Fig. 2).

In addition, the proton pump in the metabolizing cells may also facilitate the adsorption of Mg^{2+}. Microbes can exude H^+ out of the lipid bilayer using the proton pump (Kenward et al., 2013), which resisted the deprotonation of some functional groups on the cell surface, especially carboxyl and phosphate. Deprotonated carboxyl (Wang et al., 2009) and phosphate (Lambert et al., 1975a) prefer to bind to Ca^{2+} rather than Mg^{2+}. Therefore, it can be proposed that the release of H^+ to the outside of the cell would reduce the advantage of Ca^{2+} binding with carboxyl. As a result, this may favor the acceleration of Mg^{2+} on the cell surface. When the cells are dead, the advantage of Ca^{2+} binding to the organisms cannot be restrained, resulting in relatively low Mg/Ca ratios.

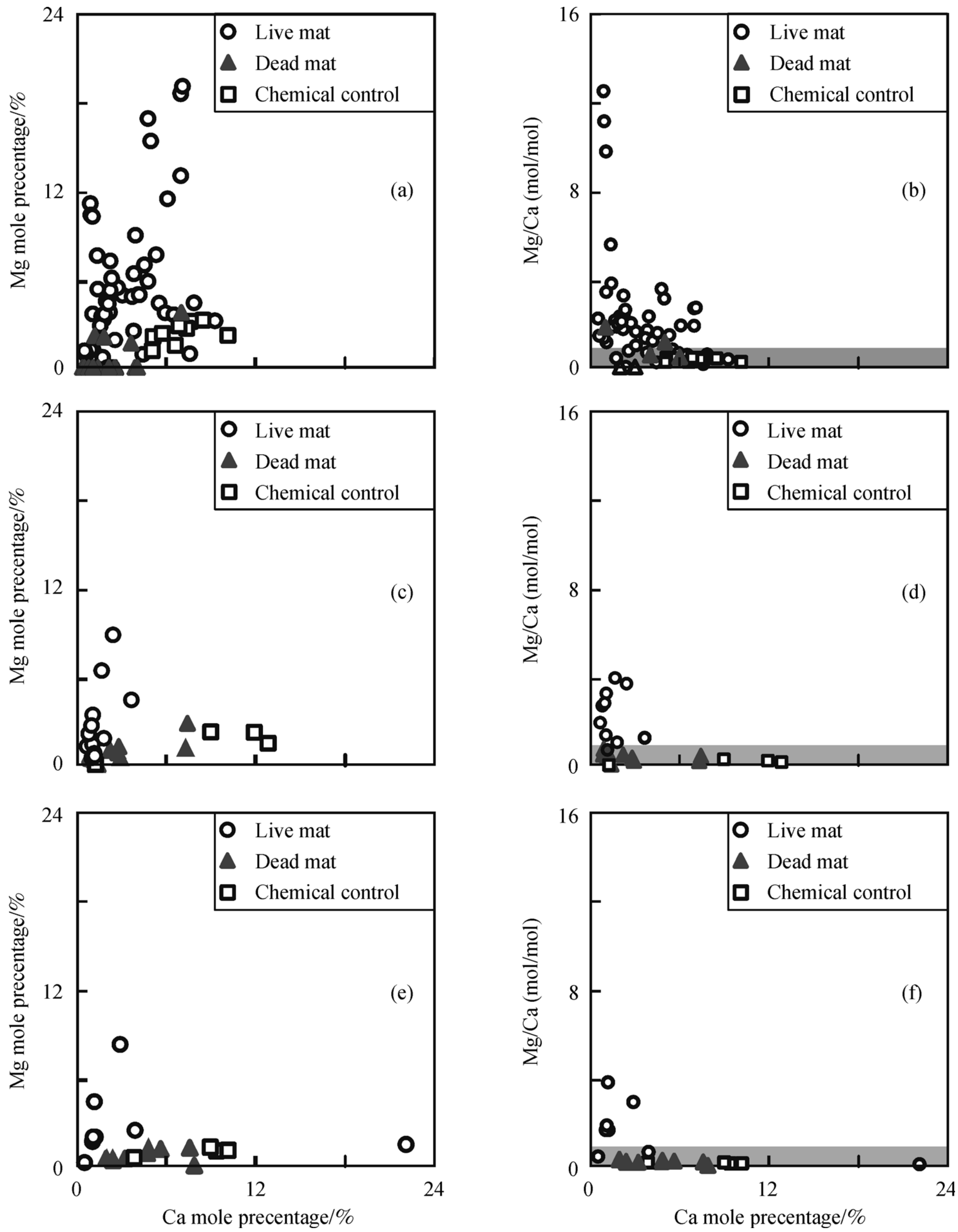

Fig. 2 The Mg^{2+} and Ca^{2+} percentages ((a), (c), and (e)) and the ratios of Mg/Ca ((b), (d), and (f)) adsorbed by microbial mats in media with different initial Mg/Ca ratios. The Mg/Ca ratio of the medium was 5.2, 2.5, and 1.5 for (a) and (b), (c) and (d), and (e) and (f), respectively. The gray areas indicate Mg/Ca ratios < 1.0.

4.2 The functional groups constrain the adsorption of Mg^{2+} and Ca^{2+}

Both the microbial cell wall and EPS can serve as the binding sites for cations due to the abundant functional groups on their surface. The carboxyl groups showed the highest capacity for cation binding (Beveridge and Murray, 1980), and phosphate groups were also found to be effective (Sakaguchi and Nakajima, 1982). Bivalent Mg^{2+} and Ca^{2+} are usually competitors for binding with functional groups. However, compared with Mg^{2+}, Ca^{2+} was reported as preferable for teichoic acid (Lambert et al., 1975a, b), lipoteichoic acid (Keith and Hogg, 1995), and amino acids (Wang et al., 2009). This indicates that the affinity of carboxyl to Ca^{2+} is higher than to Mg^{2+}.

In this study, we demonstrated that carboxyl and phosphoryl were abundant (83.08%) in the EPS of *S. elongatus* (Table 2), which resulted in higher amounts of adsorbed Ca^{2+} than Mg^{2+}. In contrast, amine was dominant (87.24%) on the cell surface of *S. elongatus* (Table 2), which caused higher amounts of adsorbed Mg^{2+} than Ca^{2+}. The results of our work are similar to that of Wilson et al.

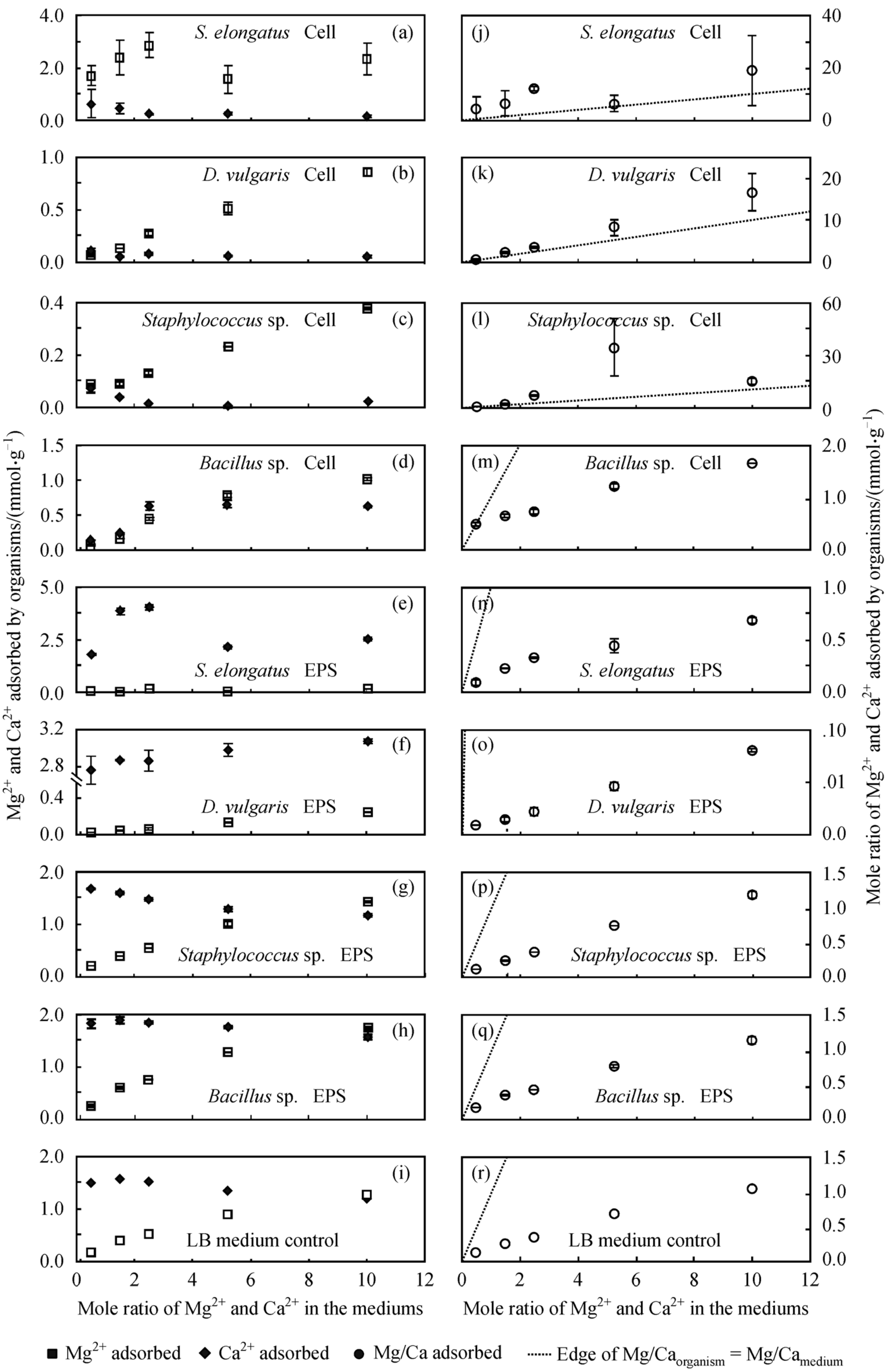

Fig. 3 Mg^{2+} and Ca^{2+} adsorbed by the cell and EPS in media with different Mg/Ca ratios. The dotted lines in the right column are the boundaries of the Mg/Ca ratio adsorbed by the organism equal to that in the original medium. The error bars from duplicate samples are shown unless they are smaller than the captions.

Table 2 Functional groups on the cell surface and EPS of *S. elongatus*

Sample	log*K* a)	log*C* b)	*C* b)	Functional groups	Percentage/%
EPS	−3.74	0.04	1.10	Carboxyl	15.11
	−7.37	0.69	4.93	Phosphoryl	67.97
	−9.12	0.09	1.23	Amine	16.92
Cell	−3.97	−0.18	0.66	Carboxyl	6.26
	−6.13	−0.17	0.68	Phosphoryl	6.50
	−8.34	0.96	9.14	Amine	87.24

Note: a) isoelectric point and b) concentration (mmol/kg).

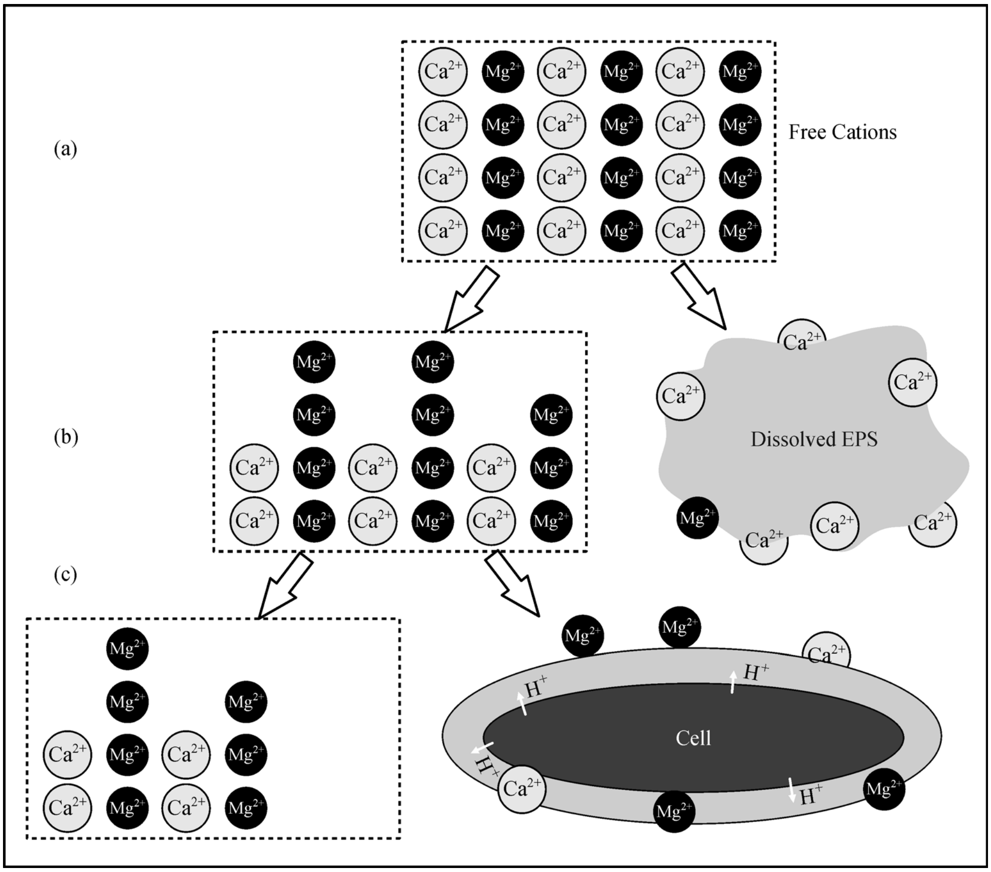

Fig. 4 Model of the allocation of Mg^{2+} and Ca^{2+} in cell–EPS–water system. (a) First stage; (b) second stage: Ca^{2+} is cheated, results in rising of the Mg/Ca ratio in the solution; (c) third stage: high Mg/Ca ratio on the cell surfaces.

(2001), who found that EPS had more acidic functional groups than basic functional groups, which may account for the large adsorption capacity of Ca^{2+}.

4.3 Releasing EPS into water facilitates the adsorption of Mg^{2+} by the cell surface

We propose that the allocation of Mg^{2+} and Ca^{2+} in the cell–EPS–water system goes through three stages. In the first stage, cations are freely dispersed in the water with few microbial cells. In the second stage, the proliferation of the microbes coupled with the release of EPS provides chelating agents for the cations in the water. In the third stage, Ca^{2+} is then largely chelated by EPS, resulting in the elevation of the ratio of free Mg^{2+} to Ca^{2+} in the water, which benefits both the chelation of Mg^{2+} on the cells and the maintenance of their high Mg/Ca ratio (Fig. 4).

Microbes commonly secrete EPS and release them into the water during their growth (De Philippis and Vincenzini, 1998). These EPS can serve as a significant Ca^{2+} sink through cation binding due to the large fraction of EPS in the total biomass (Moreno et al., 1998; Goto et al., 1999; Acuña et al., 2006) and abundant acidic functional groups on the EPS surface (Wilson et al., 2001). The binding of

Ca^{2+} by EPS will consequently increase the ratio of free Mg^{2+} to free Ca^{2+} in the solution and benefits the binding of Mg^{2+} onto the cell surface and the maintenance of the high Mg/Ca ratio of the cell. Environmental conditions control microbial diversity and the yield of the cell and EPS. The variation of the total biomass (cell and EPS) and the yield ratio of the cell and EPS may alter the ratio of Mg/Ca in the water, especially in closed locations, such as lagoons and lakes during certain periods without sufficient water exchange, or in open areas with heavy microbe blooms, such as a cyanobacterial bloom. The frequent appearance of high Mg-calcite and dolomite in lagoons and salty lakes (McKenzie and Vasconcelos, 2009) may be related to the preferential adsorption of Ca^{2+} by abundant EPS.

5 Conclusions

During the growth of microbes and microbial mats, Mg^{2+} and Ca^{2+} are adsorbed to the cell surface and dissolved EPS. More Mg^{2+} is chelated on live cells than on lifeless organic matter, regardless of the variation of the Mg/Ca ratio in the solution. The relatively few acidic functional groups located on the cell surface compared to EPS and the transport of H^+ to the outer membrane of the live cell are the potential reasons for the larger adsorption capacities of Mg^{2+} compared with lifeless organic matter. Our results may aid in understanding the mechanisms of the microbial-mediated formation of Mg-bearing carbonate minerals.

Acknowledgements We greatly thank Man Lu for her help with the titration work. This study was jointly supported by the National Natural Science Foundation of China (Grant Nos. 41130207 and 41502317), the Special Funds for Basic Scientific Research of Central Colleges, China University of Geosciences (Wuhan) (CUG120103), and the open research program from the State Key Laboratory of Biogeology and Environmental Biology (GBL21503).

References

Acuña N, Ortega-Morales B O, Valadez-González A (2006). Biofilm colonization dynamics and its influence on the corrosion resistance of austenitic UNS S31603 stainless steel exposed to Gulf of Mexico seawater. Mar Biotechnol (NY), 8(1): 62–70

Baker P A, Burns S J (1985). Occurrence and formation of dolomite in organic-rich continental margin sediments. AAPG Bull, 69(11): 1917–1930

Beveridge T, Murray R (1980). Sites of metal deposition in the cell wall of *Bacillus subtilis*. J Bacteriol, 141(2): 876–887

Bontognali T R, McKenzie J A, Warthmann R J, Vasconcelos C (2014). Microbially influenced formation of Mg-calcite and Ca-dolomite in the presence of exopolymeric substances produced by sulphate-reducing bacteria. Terra Nova, 26(1): 72–77

Bosak T, Newman D K (2003). Microbial nucleation of calcium carbonate in the Precambrian. Geology, 31(7): 577–580

Braissant O, Decho A W, Dupraz C, Glunk C, Przekop K M, Visscher P T (2007). Exopolymeric substances of sulfate-reducing bacteria: interactions with calcium at alkaline pH and implication for formation of carbonate minerals. Geobiology, 5(4): 401–411

Camoin G F, Gautret P, Montaggioni L F, Cabioch G (1999). Nature and environmental significance of microbialites in Quaternary reefs: the Tahiti paradox. Sediment Geol, 126(1−4): 271–304

Chave K, Deffeyes K, Weyl P, Garrels R, Thompson M (1962). Observations on the solubility of skeletal carbonates in aqueous solutions. Science, 137(3523): 33–34

Clapham D E (2007). Calcium Signaling. Cell, 131(6): 1047–1058

De Philippis R, Vincenzini M (1998). Exocellular polysaccharides from cyanobacteria and their possible applications. FEMS Microbiol Rev, 22(3): 151–175

Dickson J A D (2002). Fossil echinoderms as monitor of the Mg/Ca ratio of phanerozoic oceans. Science, 298(5596): 1222–1224

Folk R L, Land L S (1975). Mg/Ca ratio and salinity: two controls over crystallization of dolomite. AAPG Bull, 59(1): 60–68

Goto N, Kawamura T, Mitamura O, Terai H (1999). Importance of extracellular organic carbon production in the total primary production by tidal-flat diatoms in comparison to phytoplankton. Mar Ecol Prog Ser, 190: 289–295

Groisman E A, Hollands K, Kriner M A, Lee E J, Park S Y, Pontes M H (2013). Bacterial Mg^{2+} homeostasis, transport, and virulence. Annu Rev Genet, 47(1): 625–646

Keith R R, Hogg S D (1995). Competitive binding of calcium and magnesium to streptococcal lipoteichoic acid. BBA-Gen Subjects, 1245(1): 94–98

Kenward P A, Fowle D A, Goldstein R H, Ueshima M, González L A, Roberts J A (2013). Ordered low-temperature dolomite mediated by carboxyl-group density of microbial cell walls. AAPG Bull, 97(11): 2113–2125

Krause S, Liebetrau V, Gorb S, Sanchez-Roman M, McKenzie J A, Treude T (2012). Microbial nucleation of Mg-rich dolomite in exopolymeric substances under anoxic modern seawater salinity: new insight into an old enigma. Geology, 40(7): 587–590

Lambert P A, Hancock I C, Baddiley J (1975a). Influence of alanyl ester residues on the binding of magnesium ions to teichoic acids. Biochem J, 151(3): 671–676

Lambert P A, Hancock I C, Baddiley J (1975b). The interaction of magnesium ions with teichoic acid. Biochem J, 149(3): 519–524

Land L S (1998). Failure to precipitate dolomite at 25°C from dilute solution despite 1000-fold oversaturation after 32 years. Aquat Geochem, 4(3): 361–368

Liu D, Dong H, Bishop M E, Zhang J, Wang H, Xie S, Wang S, Huang L, Eberl D D (2012). Microbial reduction of structural iron in interstratified illite-smectite minerals by a sulfate-reducing bacterium. Geobiology, 10(2): 150–162

McKenzie J A, Vasconcelos C (2009). Dolomite Mountains and the origin of the dolomite rock of which they mainly consist: historical developments and new perspectives. Sedimentology, 56(1): 205–219

Michiels J, Xi C, Verhaert J, Vanderleyden J (2002). The functions of Ca^{2+} in bacteria: a role for EF-hand proteins? Trends Microbiol, 10 (2): 87–93

Moreno J, Vargas M, Olivares H, Rivas J N, Guerrero M G (1998). Exopolysaccharide production by the cyanobacterium *Anabaena* sp.

ATCC 33047 in batch and continuous culture. J Biotechnol, 60(3): 175–182

Mucci A, Morse J W (1983). The incorporation of Mg^{2+} and Sr^{2+} into calcite overgrowths: influences of growth rate and solution composition. Geochim Cosmochim Acta, 47(2): 217–233

Qiu X, Wang H M, Liu D, Gong L F, Wu X P, Xiang X (2012). The physiological response of *Synechococcus elongatus* to salinity: a potential biomarker for ancient salinity in evaporative environments. Geomicrobiol J, 29(5): 477–483

Reeder R J, Sheppard C E (1984). Variation of lattice parameters in some sedimentary dolomites. Am Mineral, 69(5−6): 520–527

Ries J B, Anderson M A, Hill R T (2008). Seawater Mg/Ca controls polymorph mineralogy of microbial $CaCO_3$: a potential proxy for calcite-aragonite seas in Precambrian time. Geobiology, 6(2): 106–119

Sakaguchi T, Nakajima A (1982). Recovery of uranium by chitin phosphate and chitosan phosphate. Proceedings of the 2nd International Conference on Chitin and Chitosan, 177–182

Sandberg P A (1983). An oscillating trend in Phanerozoic non-skeletal carbonate mineralogy. Nature, 305(5929): 19–22

Saunders P, Rogerson M, Wadhawan J D, Greenway G, Pedley H M (2014). Mg/Ca ratios in freshwater microbial carbonates: thermodynamic, kinetic and vital effects. Geochim Cosmochim Acta, 147: 107–118

Spadafora A, Perri E, McKenzie J A, Vasconcelos C (2010). Microbial biomineralization processes forming modern Ca:Mg carbonate stromatolites. Sedimentology, 57(1): 27–40

Stoupin D, Kiss A K, Arndt H, Shatilovich A V, Gilichinsky D A, Nitsche F (2012). Cryptic diversity within the choanoflagellate morphospecies complex *Codosiga botrytis*–Phylogeny and morphology of ancient and modern isolates. Eur J Protistol, 48(4): 263–273

Turner B F, Fein J B (2006). Protofit: a program for determining surface protonation constants from titration data. Comput Geosci, 32(9): 1344–1356

Van Lith Y, Warthmann R, Vasconcelos C, McKenzie J A (2003). Microbial fossilization in carbonate sediments: a result of the bacterial surface involvement in dolomite precipitation. Sedimentology, 50(2): 237–245

Wang D B, Wallace A F, De Yoreo J J, Dove P M (2009). Carboxylated molecules regulate magnesium content of amorphous calcium carbonates during calcification. Proc Natl Acad Sci USA, 106(51): 21511–21516

Wilson W W, Wade M M, Holman S C, Champlin F R (2001). Status of methods for assessing bacterial cell surface charge properties based on zeta potential measurements. J Microbiol Methods, 43(3): 153–164

Xu J, Yan C, Zhang F F, Konishi H, Xu H F, Teng H H (2013). Testing the cation-hydration effect on the crystallization of Ca–Mg–CO_3 systems. Proc Natl Acad Sci USA, 110(44): 17750–17755